Scanning paraxial optical tomography

Vadim A. Markel and John C. Schotland

Department of Radiology, Washington University, St. Louis, Missouri 63110

Received January 31, 2002

We present a solution to this problem in the form of a fast algorithm with computational complexity that scales as $N \log N$, where N is the number of spatial measurements of the scattered field. © 2002 Optical Society of America

OCIS codes: 170.6960, 290.3200.

There has been considerable recent interest in the development of tomographic methods for imaging with diffuse light.[1] Such methods have the potential to provide novel diagnostic tools while complementing existing medical imaging modalities. Clinical applications of current importance include breast imaging and functional brain mapping. A typical experimental configuration, often used in optical mammography,[2,3] is the slab geometry in which N harmonically modulated point sources are located on one face of the slab and N point detectors are located on the opposite face [Fig. 1(c)]. The physical problem to be considered consists of reconstructing the optical properties of the interior of the slab from a complete set of N^2 measurements taken on its surface. It is often assumed that many measurements (at a fixed modulation frequency) are needed for obtaining images with high spatial resolution, a requirement that is difficult to realize in practice. Such large data sets also lead to image reconstruction algorithms with high computational complexity. Thus the development of reconstruction algorithms that are both computationally efficient and reduce the required number of spatial measurements below $O(N^2)$ would be of considerable importance.

To mitigate the principal difficulties associated with the complete-data problem, we consider the problem in the paraxial geometry. In this geometry a single source is used to illuminate the medium, and the scattered light is collected by an on-axis detector along with a small number of off-axis detectors [Fig. 1(b)]. The entire source–detector array is then scanned over N points on the surface of the slab while the frequency of the source is varied over a specified range, resulting in $O(N)$ spatial measurements. We refer to this method as scanning paraxial optical tomography. In this Letter we show that the linearized form of the corresponding inverse scattering problem may be solved analytically by means of an explicit inversion formula. This result has three important consequences. First, by trading spatial information for frequency information, we obtain an image reconstruction algorithm that reduces the required number of spatial measurements of the scattered field from $O(N^2)$ to $O(N)$. Evidently, this reduction leads to a considerable simplification of the imaging experiment. Second, this algorithm has computational complexity that scales as $N \log N$ and is stable in the presence of added noise. This result should be compared with the $N^2 \log N$ scaling of the computational complexity of the complete-data problem.[4] Third, we explicitly account for the effects of sampling of the data, obtaining reconstructed images whose spatial resolution scales as the minimum separation between the sources.

We begin by considering the propagation of diffuse light in the slab geometry. For simplicity, we assume that the slab is characterized by an inhomogeneous optical absorption coefficient $\alpha(\mathbf{r})$ and a diffusion constant D_0. The change in intensity of transmitted light as a result of fluctuations in $\alpha(\mathbf{r})$ is given by the integral equation[5]

$$\phi(\boldsymbol{\rho}_1, \boldsymbol{\rho}_2) = \int \mathrm{d}^3 r \Gamma(\boldsymbol{\rho}_1, \boldsymbol{\rho}_2; \mathbf{r}) \delta\alpha(\mathbf{r}). \quad (1)$$

Here, the data function $\phi(\boldsymbol{\rho}_1, \boldsymbol{\rho}_2)$ is proportional to the change in complex intensity relative to a reference medium with absorption α_0, $\delta\alpha(\mathbf{r}) = \alpha(\mathbf{r}) - \alpha_0$, and $\boldsymbol{\rho}_1$ and $\boldsymbol{\rho}_2$ denote the transverse coordinates of the source and the detector, respectively. The kernel $\Gamma(\boldsymbol{\rho}_1, \boldsymbol{\rho}_2; \mathbf{r})$ may be obtained from the Green's function for the diffusion equation in the reference medium and is given by the plane-wave decomposition:

$$\Gamma(\boldsymbol{\rho}_1, \boldsymbol{\rho}_2; \mathbf{r}) = \frac{1}{(2\pi)^4} \int \mathrm{d}^2 q_1 \mathrm{d}^2 q_2 \kappa(\mathbf{q}_1, \mathbf{q}_2; z) \times \exp[-i(\mathbf{q}_1 - \mathbf{q}_2) \cdot \mathbf{r}_\perp + i(\mathbf{q}_1 \cdot \boldsymbol{\rho}_1 - \mathbf{q}_2 \cdot \boldsymbol{\rho}_2)], \quad (2)$$

where $\mathbf{r} = (\mathbf{r}_\perp, z)$. General expressions for $\kappa(\mathbf{q}_1, \mathbf{q}_2; z)$ are given in Ref. 5 and depend on the nature

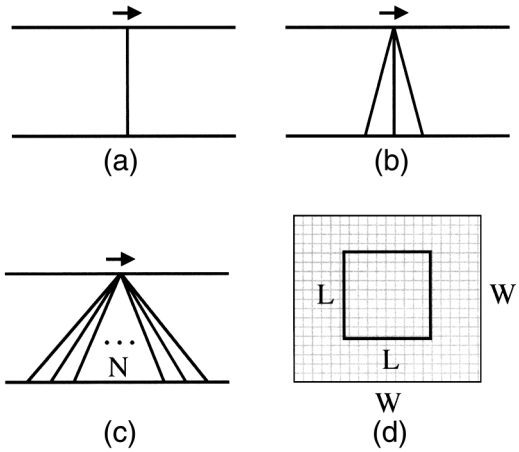

Fig. 1. Illustration of the geometries corresponding to the (a) axial, (b) paraxial, and (c) complete-data problems. Also illustrated in (d) is the relationship between the window size, W, and the linear dimension of the field of view, L.

0146-9592/02/131123-03$15.00/0

of the boundary conditions obeyed by the Green's function. Here we restrict our attention to absorbing boundary conditions, in which case $\kappa(\mathbf{q}_1, \mathbf{q}_2; z)$ is of the form

$$\kappa(\mathbf{q}_1, \mathbf{q}_2; z) = \frac{\sinh[Q(q_1)(L - z)]\sinh[Q(q_2)z]}{\sinh[Q(q_1)L]\sinh[Q(q_2)L]}, \quad (3)$$

where L is the slab thickness and $Q(q) = [q^2 + k^2(\omega)]^{1/2}$; $k^2(\omega) = (\alpha_0 - i\omega)/D_0$ is the diffuse wave number at the source modulation frequency, ω.

In the paraxial geometry we denote the transverse coordinate of the source by $\boldsymbol{\rho}$, and we assume that the detectors have transverse coordinates $\boldsymbol{\rho} + \delta\boldsymbol{\rho}_n$, where the off-axis displacement of the nth detector, $\delta\boldsymbol{\rho}_n$, is assumed to be sufficiently small, $|\delta\boldsymbol{\rho}_n| \ll L$. We further assume that linear combinations of detector outputs of the form $\psi_n(\boldsymbol{\rho}) = \sum_m c_{nm}\phi(\boldsymbol{\rho}, \boldsymbol{\rho} + \delta\boldsymbol{\rho}_m)$ are directly measurable. The coefficients c_{nm} are taken to be complex, allowing for the possibility of a phased-array measurement scheme. Making use of these definitions, we find that integral equation (1) becomes

$$\psi_n(\boldsymbol{\rho}) = \int \mathrm{d}^3 r \sum_m c_{nm}\Gamma(\boldsymbol{\rho}, \boldsymbol{\rho} + \delta\boldsymbol{\rho}_m; \mathbf{r})\delta\alpha(\mathbf{r}). \quad (4)$$

We now observe that, when the modulation frequency of the source is fixed, the inverse problem of reconstructing $\delta\alpha(\mathbf{r})$ from $\psi_n(\boldsymbol{\rho})$ is underdetermined. This should be contrasted with the complete-data inverse problem defined by Eq. (1), which is overdetermined. The overdetermined nature of the complete-data problem is the origin of the requirement for $O(N^2)$ measurements of the scattered field. In the paraxial geometry, however, we show that by varying the modulation frequency it is possible to include sufficient additional information to allow the inverse problem to be solved uniquely, requiring only $O(N)$ spatial measurements.

A special case of the paraxial geometry is the axial geometry shown in Fig. 1(a). We note that in the absence of off-axis data there is still, in principle, sufficient information to solve the inverse problem (with multiple frequencies). However, in this case a symmetry is present in integral equation (4). This symmetry is manifested by the invariance of $\phi(\boldsymbol{\rho}, \boldsymbol{\rho})$ under reflection of $\delta\alpha(\mathbf{r})$ about the midplane of the slab. Thus, reconstructions based on axial data contain twin reflected images of $\delta\alpha(\mathbf{r})$. To eliminate such artifacts it is necessary to break the reflection symmetry. This can be achieved by introduction of additional data in the form of paraxial measurements.

We now consider the derivation of the inversion formula for scanning paraxial optical tomography. To account for sampling of the data, we assume that $\psi_n(\boldsymbol{\rho})$ is measured on a two-dimensional square lattice with lattice spacing a. It will prove useful to introduce the Fourier transform of $\psi_n(\boldsymbol{\rho})$, which is defined by $\hat{\psi}_n(\mathbf{q}) = \sum_{\boldsymbol{\rho}} \exp(i\mathbf{q} \cdot \boldsymbol{\rho})\psi_n(\boldsymbol{\rho})$, where the sum over $\boldsymbol{\rho}$ is carried out over all lattice vectors. Here, $\mathbf{q}$ belongs to the first Brillouin zone (FBZ) of the lattice. Making use of Eq. (4) and the identity $\sum_\rho \exp(i\mathbf{q} \cdot \boldsymbol{\rho}) = (2\pi/a)^2 \sum_{\mathbf{p}} \delta(\mathbf{q} - \mathbf{p})$, where $\mathbf{p}$ denotes a reciprocal lattice vector, we arrive at the system of equations

$$\hat{\psi}_n(\omega; \mathbf{q}) = \int_0^L \mathrm{d}z \sum_{\mathbf{p}} K_n(\omega, z; \mathbf{q} - \mathbf{p})\widetilde{\delta\alpha}(\mathbf{q} - \mathbf{p}, z), \quad (5)$$

where

$$K_n(\omega, z; \mathbf{q}) = \int \frac{\mathrm{d}^2 q'}{(2\pi a)^2} \sum_m c_{nm}\kappa(\mathbf{q}' + \mathbf{q}, \mathbf{q}'; z) \times \exp(i\mathbf{q}' \cdot \delta\boldsymbol{\rho}_m), \quad (6)$$

$\widetilde{\delta\alpha}(\mathbf{q}, z) = \int \mathrm{d}^2 r_\perp \exp(i\mathbf{q} \cdot \mathbf{r}_\perp)\delta\alpha(\mathbf{r})$, the dependence of all quantities on modulation frequency ω has been made explicit, and the integration over $\mathbf{q}'$ is over all space. For fixed $\mathbf{q}$, Eq. (5) defines a system of one-dimensional integral equations for $\widetilde{\delta\alpha}(\mathbf{q}, z)$. Following the general method of Ref. 4 we find that the pseudoinverse solution of Eq. (5) is given by

$$\widetilde{\delta\alpha}(\mathbf{q} - \mathbf{p}, z) = \sum_{\omega, \omega'} \sum_{n, m} K_n{}^*(\omega, z; \mathbf{q} - \mathbf{p}) \times M_{nm}{}^{-1}(\omega, \omega'; \mathbf{q})\hat{\psi}_m(\omega', \mathbf{q}), \quad (7)$$

where the frequencies ω and ω' are treated as discrete and $M_{nm}(\omega, \omega'; \mathbf{q})$, which is to be interpreted as a block matrix, is given by the overlap integral

$$M_{nm}(\omega, \omega'; \mathbf{q}) = \int_0^L \mathrm{d}z \sum_{\mathbf{p}} K_n(\omega, z; \mathbf{q} - \mathbf{p}) \times K_m{}^*(\omega', z; \mathbf{q} - \mathbf{p}). \quad (8)$$

Since all possible transverse Fourier components of $\delta\alpha(\mathbf{r})$ are specified by Eq. (7), we may apply the inverse Fourier transform to arrive at the inversion formula

$$\delta\alpha(\mathbf{r}) = \int_{\mathrm{FBZ}} \frac{\mathrm{d}^2 q}{(2\pi)^2} \exp(-i\mathbf{q} \cdot \mathbf{r}_\perp) \sum_{\omega, \omega'} \sum_{n, m} \sum_{\mathbf{p}} \times \exp(i\mathbf{p} \cdot \mathbf{r}_\perp) K_n{}^*(\omega, z; \mathbf{q} - \mathbf{p}) \times M_{nm}{}^{-1}(\omega, \omega'; \mathbf{q})\hat{\psi}_m(\omega', \mathbf{q}), \quad (9)$$

which is the main result of this Letter.

Several comments on inversion formula (9) are necessary. First, the solution that we have constructed to the inverse problem of scanning paraxial optical tomography is the unique minimum L^2 norm solution to integral equation (4).[4] Second, the required number of spatial measurements of the scattered field is $O(N)$ rather than $O(N^2)$ as in the complete-data problem. Third, with the use of the fast Fourier transform to compute $\hat{\psi}_n(\mathbf{q})$, a reconstruction algorithm based on Eq. (9) has computational complexity that scales as $N \log N$. Fourth, if $\delta\alpha(\mathbf{r})$ is assumed to be transversely band limited, then the sum over $\mathbf{p}$ in Eqs. (8) and (9) may be truncated. In this situation the inversion formula produces the best (in the sense of minimizing the L^2 norm) band-limited

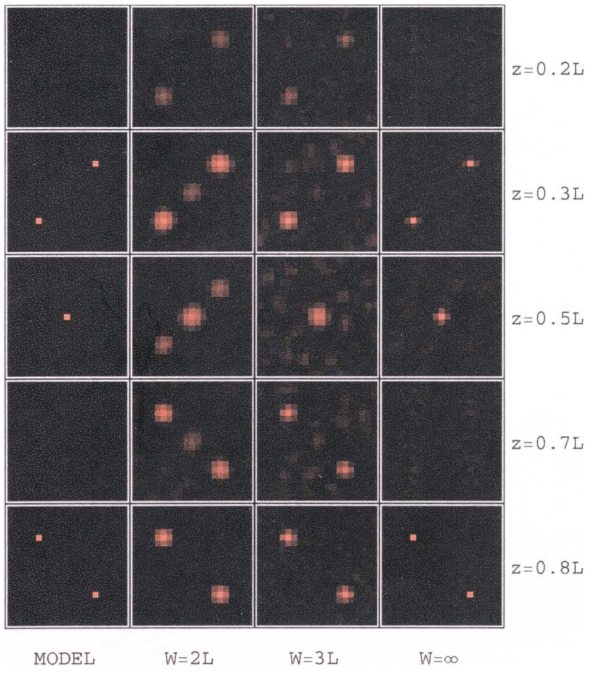

Fig. 2. Tomographic images of the slab at different depths z and window sizes W. The images are calibrated from -1 (blue) to 1 (red) all on the same linear color scale. Here red corresponds to the maximum value of $\delta\alpha$ obtained for a point absorber located in the center of the field of view at a particular depth.

approximation to $\delta\alpha(\mathbf{r})$ that is consistent with the lattice on which $\psi_n(\boldsymbol{\rho})$ is sampled. Fifth, to avoid numerical instability and control the ill-posedness of the inverse problem, M^{-1} must be regularized to limit the contribution of small singular values of M. The simplest way to do this is to ignore all singular values below some threshold ϵ. The minimum value of ϵ for which the reconstruction algorithm is numerically stable is defined by experimental noise and in the absence of noise by numerical precision. Sixth, the speed of data collection may be further increased by employment of multiple frequency-encoded sources. Finally, our results may be extended to the paraxial cylindrical geometry and also to the problem of simultaneous reconstruction of both the absorption and diffusion coefficients in either the slab or cylindrical geometries.

Multiple factors influence the spatial resolution of images reconstructed with inversion formula (9). In the absence of noise, the transverse resolution is controlled by the size of the FBZ and is therefore equal to the lattice spacing, a. In the presence of noise, for sufficiently small values of the regularization parameter, ϵ, the transverse resolution still scales as a. However, resolution in the depth direction is a different matter and is primarily determined by numerical precision. Resolution is further influenced by limiting the size of the window W on which the data function $\psi_n(\boldsymbol{\rho})$ is sampled [Fig. 1(d)]. Smaller values of W require larger values of ϵ to stabilize the reconstruction, resulting in a corresponding decrease in the resolution.

To illustrate the use of inversion formula (9), we have numerically simulated the reconstruction of $\delta\alpha(\mathbf{r})$ for one or more point absorbers of the form $\delta\alpha(\mathbf{r}) = A\delta(\mathbf{r} - \mathbf{r}_0)$, with $A = 2\ \mathrm{cm}^3\ \mathrm{ns}^{-1}$. In this situation the data function $\psi_n(\boldsymbol{\rho})$ may be obtained in closed form. The simulations were performed for a slab of thickness $L = 5$ cm with optical properties similar to breast tissue in the near infrared. The background absorption and diffusion coefficients are given by $\mu_a = \alpha_0/c = 0.03\ \mathrm{cm}^{-1}$ and $D_0 = 0.4\ \mathrm{cm}^2\ \mathrm{ns}^{-1}$. Three linear paraxial detectors were used, as shown in Fig. 1(b), with $|\delta\boldsymbol{\rho}_n| = 2na$ for $n = 0, 1$. The outputs of the two outer detectors are added so that the corresponding coefficients c_{nm} are set equal to unity, with all other matrix elements vanishing. The source–detector array is scanned over a square lattice of size $W \times W$ with lattice spacing $a = 0.25$ cm. Fifteen uniformly spaced modulation frequencies over the range $0 \leq \omega/2\pi \leq 1$ GHz are employed. Numerical integration over $\mathbf{q}$ is carried out over a 41×41 square grid in the FBZ. The field of view of each reconstructed image is $L \times L$, with the pixel size coinciding with the lattice spacing, a.

In Fig. 2 we present reconstructions at different depths of several point absorbers located in the planes $z = 0.3L$, $z = 0.5L$, and $z = 0.8L$. To demonstrate the stability of the reconstruction algorithm in the presence of noise, we added Gaussian noise of zero mean to the data at the 1% level, relative to the mean signal, for $W = 2L$ and $W = 3L$. The regularization parameter, ϵ, was taken to be $\epsilon = 10^{-9}$ for $W = 2L$, $\epsilon = 10^{-10}$ for $W = 3L$, and $\epsilon = 10^{-18}$ for $W = \infty$. It can be seen that as the window size is increased from $W = 2L$ to $W = 3L$ the resolution of the reconstructed images improves. This improvement continues until, in the absence of noise, for an infinite window the fundamental limit of transverse resolution is achieved. Note the absence of twin reflected images in the planes $z = 0.2L$ and $z = 0.7L$. To translate these results to the clinical setting, we note for a window size of $W = 15$ cm, corresponding to $N = (W/a)^2 = 3600$ measurements, that a resolution of 2.5–5.0 mm should be achievable depending on the level of noise.

In conclusion, we have described a fast image reconstruction algorithm for optical tomography in the paraxial geometry. This algorithm achieves high spatial resolution while simultaneously reducing the required number of independent spatial measurements of the scattered field.

References

1. S. Arridge, Inv. Prob. **15,** R41 (1999).
2. M. Franceschini, K. Moesta, S. Fantini, G. Gaida, E. Gratton, H. Jess, W. Mantulin, M. Seeber, P. Schlag, and M. Kaschke, Proc. Natl. Acad. Sci. USA **94,** 6468 (1997).
3. V. Ntziachristos, A. Yodh, M. Schnall, and B. Chance, Proc. Natl. Acad. Sci. USA **97,** 2769 (1999).
4. V. Markel and J. Schotland, Phys. Rev. E **64,** 035601(R) (2001).
5. V. Markel and J. Schotland, J. Opt. Soc. Am. A **19,** 558 (2002).